

# JGR Biogeosciences



## RESEARCH ARTICLE

10.1029/2019JG005505

### Special Section:

The Arctic: An AGU Joint Special Collection

## Spatial Variability of Dissolved Organic Carbon, Solutes, and Suspended Sediment in Disturbed Low Arctic Coastal Watersheds

C. Coch<sup>1,2,3</sup> , J. L. Ramage<sup>2,3,4</sup> , S. F. Lamoureux<sup>5</sup> , H. Meyer<sup>2</sup>, C. Knoblauch<sup>6,7</sup> , and H. Lantuit<sup>2,3</sup> 

### Key Points:

- Between 1952 and 2015, the total disturbed area decreased by 41%, and the number of disturbances increased by 66%
- Hydrological connectivity of permafrost disturbances is essential to impact suspended sediment and solute concentrations in the stream
- There is a linear relationship between catchment size and daily flux of dissolved organic carbon, total dissolved nitrogen, and solutes

### Supporting Information:

- Supporting Information S1

### Correspondence to:

C. Coch,  
 coch.caroline@gmail.com

### Citation:

Coch, C., Ramage, J. L., Lamoureux, S. F., Meyer, H., Knoblauch, C., & Lantuit, H. (2020). Spatial variability of dissolved organic carbon, solutes, and suspended sediment in disturbed Low Arctic coastal watersheds. *Journal of Geophysical Research: Biogeosciences*, 125, e2019JG005505. <https://doi.org/10.1029/2019JG005505>

Received 5 OCT 2019

Accepted 29 JAN 2020

Accepted article online 3 FEB 2020

<sup>1</sup>The Living Planet Centre, World Wildlife Fund, Woking, UK, <sup>2</sup>Alfred Wegener Institute Helmholtz Centre for Polar and Marine Research, Potsdam, Germany, <sup>3</sup>Institute for Geosciences, University of Potsdam, Potsdam, Germany, <sup>4</sup>Nordregio, Stockholm, Sweden, <sup>5</sup>Department of Geography and Planning, Queen's University, Kingston, Ontario, Canada, <sup>6</sup>Institute of Soil Science, Universität Hamburg, Hamburg, Germany, <sup>7</sup>Center for Earth System Research and Sustainability, Universität Hamburg, Hamburg, Germany

**Abstract** Climate change in the Arctic leads to permafrost degradation and to associated changes in freshwater geochemistry. There is a limited understanding of how disturbances such as active layer detachments or retrogressive thaw slumps impact water quality on a catchment scale. This study investigates how permafrost degradation affects concentrations of dissolved organic carbon (DOC), total dissolved solids (TDS), suspended sediment, and stable water isotopes in adjacent Low Arctic watersheds. We incorporated data on disturbance between 1952 and 2015, as well as sporadic runoff and geochemistry data of streams nearby. Our results show that the total disturbed area decreased by 41% between 1952 and 2015, whereas the total number of disturbances increased by 66% in all six catchments. The spatial variability of hydrochemical parameters is linked to catchment properties and not necessarily reflected at the outflow. Degrading ice-wedge polygons were found to increase DOC concentrations upstream in Ice Creek West, whereas hydrologically connected disturbances were linked to increases in TDS and suspended sediment. Although we found a great spatial variability of hydrochemical concentrations along the paired watershed, there was a linear relationship between catchment size and daily DOC, total dissolved nitrogen, and TDS fluxes for all six streams. Suspended sediment flux on the contrary did not show a clear relationship as one hydrologically connected retrogressive thaw slump impacted the overall flux in one of the streams. Understanding the spatial variability of water quality will help to model the lateral geochemical fluxes from Arctic catchments.

**Plain Language Summary** One effect climate change has in the Arctic is the thawing of permafrost. Permafrost is defined as ground that remains below 0 °C for at least two consecutive years. The low temperatures in the High North lead to very slow decomposition rates of organic material from plants and animals. A lot of this material has accumulated over thousands of years. As air temperatures in the Arctic are rising, permafrost is thawing. This is also termed permafrost degradation. It can occur in two forms: (1) The gradual deeper thawing of permafrost is called *thermal perturbation*. It might lead to a subsidence (sinking) of the ground, because water that was previously frozen runs off. (2) Thawing of the ground may lead to a destabilization of the ground and connected landslides. This is termed *physical or surface disturbance*. These two forms of permafrost degradation have an impact on the water quality of rivers flowing through the terrain. In this study, we investigated the impacts of permafrost degradation on stream hydrochemistry on Herschel Island, Yukon Territory, Canada. We identified active physical disturbances in the past using aerial photographs from 1952 and 1970 and satellite images from 2011 and 2015. This was done for the areas from which rainwater flows into the same river (catchment area) of six streams named Water Creek, Beach Creek, Fox Creek, Ice Creek West, Ice Creek East, and Eastern Gully. In 2016, we collected water samples along two neighboring streams (Ice Creek West and Ice Creek East) to compare the impacts of local physical disturbances on the hydrochemistry. In these two streams, we also measured water flow (discharge) during the monitoring season. We further collected samples at the outflow of the other four streams nearby. Water samples were analyzed in the laboratory for different chemical properties that help us to understand the influence of permafrost degradation. For the six streams, we found that the total disturbed area decreased by 41% between 1952 and 2015, whereas the total number of disturbances increased by 66%. We were able to link permafrost degradation to changes in chemical water

©2020. The Authors.

This is an open access article under the terms of the Creative Commons Attribution License, which permits use, distribution and reproduction in any medium, provided the original work is properly cited.

composition within the two neighboring streams. It is important that disturbances are “hydrologically connected” to impact concentrations of inorganic compounds (total dissolved solids) and mud (suspended sediment) in the streams. Essentially, this means that water needs to flow through these disturbances to mobilize the material and influence the concentration in the stream. Taking all studied streams together, the overall flux of dissolved organic carbon, total dissolved solids, and total dissolved nitrogen (i.e., the amount of chemical compound [in kg] transported away in every liter of river water) depends on catchment size. The larger the catchment, the more of this material is transported away. This relationship could not be confirmed for suspended sediment, because a hydrologically connected retrogressive thaw slump heavily impacted the flux in one of the streams. This study is important because the river water ultimately drains into the Arctic Ocean and might change the water quality there. This may have consequences for the animals and plants living in the ocean. We need to understand the influence of permafrost degradation on stream water quality to assess future changes of the Arctic Ocean.

## 1. Introduction

The temperature rise in the Arctic is about twice as fast as the global average (IPCC, 2013). This has profound consequences for the permafrost region, where ground remaining below 0 °C for at least two consecutive years can be found. Warming leads to gradual deeper thawing of the active layer (Osterkamp, 2007; M.-K. Woo et al., 2008), sometimes also referred to as thermal perturbation (Lafrenière & Lamoureux, 2019). Geomorphological or physical disturbances such as active layer detachments (ALDs) or retrogressive thaw slumps (RTSs; Lacelle et al., 2010; Lewkowicz, 2007; Ramage et al., 2017) alter surface flow pathways and deep thawing of the active layer changes subsurface pathways (Frey & McClelland, 2009; Lafrenière & Lamoureux, 2019; Vonk et al., 2015). Furthermore, permafrost deposits may contain large amounts of ice, which add substantial amounts of liquid water to degrading permafrost landscapes after thaw (Liljedahl et al., 2016). Climate models project a continued increase of warming (IPCC, 2013), which will lead to further degradation of permafrost. Bintanja and Andry (2017) also anticipate an increase of rainfall frequency and intensity across the Arctic in the future, which will impact the lateral biogeochemical fluxes (Coch et al., 2018). The understanding of the linkages between permafrost degradation and hydrology as well as the quantification of fluxes is important since the sediment and organic matter released by coastal catchments may impact the biogeochemistry of the Arctic Ocean (Wegner et al., 2015).

The release of dissolved organic carbon (DOC), solutes, and suspended sediment on a catchment scale is dependent on hydrological connectivity (Lafrenière & Lamoureux, 2013). Understanding the interplay between snowmelt, precipitation, and physical and thermal disturbances is essential to quantify lateral biogeochemical fluxes. Research from the High Arctic suggests that physical disturbances such as ALDs or thaw slumps lead to increased solute and sediment fluxes (Lamoureux & Lafrenière, 2017). They found that sediment concentrations generally recover to predisturbance conditions in approximately 5 years, while solute concentrations are impacted for more than 5 years. Thermal perturbation also enhances solute fluxes (Lafrenière & Lamoureux, 2013; Lamhonwah et al., 2017; Lamoureux & Lafrenière, 2009, 2017). The impact of RTSs, ALD slides, and thermoerosional gullies on stream biogeochemistry has also been studied on the North Slope of Alaska, where thermokarst increased concentrations of DOC, inorganic nitrogen, and solutes further downstream (Abbott et al., 2015; Bowden et al., 2008).

While current research provides an important insight on how stream biogeochemistry is altered at the outflow of thermokarst features in the Low Arctic, the impacts of those features on a catchment scale remain unknown. Concentrations at the outflow of a river can be regarded as an integrator, which reflects the conditions of an entire catchment. There is a limited understanding of how water quality is changing from upstream to downstream (Tank et al., 2018), especially with respect to present and past permafrost degradation. The objective of this study is therefore to explore the spatial heterogeneity of DOC, suspended sediment, solutes, and water isotope signatures of paired watersheds that have been subject to permafrost degradation. More specifically, we (1) assess the hydrological response and hydrochemical composition of stream water during the 2016 summer season and (2) investigate how water quality changes from the headwaters downstream. We investigate paired watersheds on Herschel Island (Yukon, Canada) in detail and extend the data set by incorporating outflow and geochemical data from nearby Arctic rivers of different sizes with catchments influenced by different degrees of disturbance.

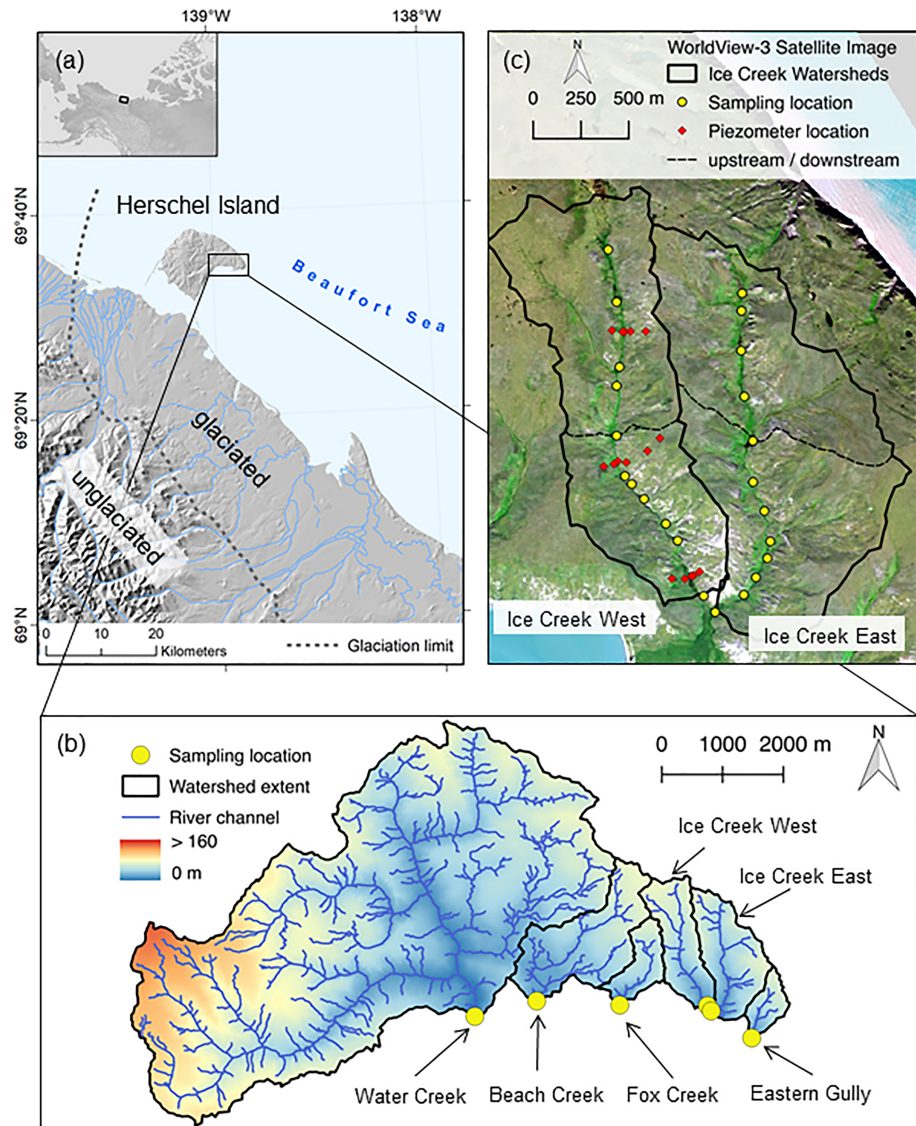


**Figure 1.** Maps showing (a) the location of Herschel Island and the glaciation limit along the Yukon coast; (b) the digital elevation model, river channels, and water sampling locations of the studied watersheds (east to west) Water Creek, Beach Creek, Fox Creek, Ice Creek West, Ice Creek East, and Eastern Gully; and (c) the detailed sampling map of the adjacent Ice Creek East and West including water sampling locations (yellow) and piezometer profiles (red) and the separation between upstream and downstream (dashed line). Projection: NAD 83/UTM zone 7N. Image Base: WorldView-3 2015 satellite image.

## 2. Study Site

Herschel Island covers an area of approximately 116 km<sup>2</sup> and is located in the Beaufort Sea off the Yukon coast of Canada at 69°35' N and 139°05' W (Figure 1a). The maximum elevation is about 180 m above sea level. The island, an ice-thrust moraine, was formed by the Laurentide Ice Sheet, and it is composed of unconsolidated and fine-grained marine and glacial sediments (Rampton, 1982). The ground ice content is estimated to be between 30% and 60% for the entire island (Mackay, 1959). Herschel Island is situated in the zone of continuous permafrost. Burn and Zhang (2009) monitored ground temperatures on the east side of the island and found the mean annual ground temperature to be −8 °C at a depth of zero annual amplitude of 14.5 m. The ice-rich permafrost leads to rapid coastal erosion and the presence of numerous RTs along the shore (Lantuit & Pollard, 2008; Radosavljevic et al., 2015). Mass wasting processes occur also in the form of ALDs, thermal erosion gullies, or solifluction affecting the soil organic carbon storage (Obu

**Table 1**

*Comparison of Catchment Properties (Area, Mean Elevation, Slope, and Aspect) for the Watersheds Water Creek, Beach Creek, Fox Creek, Ice Creek West, Ice Creek East and Eastern Gully (East to West)*

Catchment	Area (ha)	Maximum catchment elevation (m)	Mean catchment slope (°)	Mean catchment aspect (°)
Water Creek	2,678	176	6.4 ± 3.3	196 ± 89
Beach Creek	255	94	4.3 ± 3.3	207 ± 83
Fox Creek	73	83	5.7 ± 4.4	190 ± 77
Ice Creek West	138	88	5.2 ± 3.6	209 ± 68
Ice Creek East	165	95	5.3 ± 3.3	171 ± 94
Eastern Gully	44	85	5.7 ± 3.1	169 ± 84

et al., 2017). Based on the Canadian system of soil classification, organic cryosols dominate the island. Turbic cryosols and static cryosols are found on beaches and spits where near-surface permafrost is absent (Smith et al., 1989). The lowland tundra vegetation (Myers-Smith et al., 2011; Smith et al., 1989) can be classified to Subzone E (CAVM, 2003), the Low Arctic.

Environment and Climate Change Canada runs an automated weather station at Pauline Cove on the east side of Herschel Island (WMO ID: 715010) with temperature recordings since 1995. Precipitation records are only available from 2004 and often incomplete. The mean annual air temperature compiled from no-gap data months between 1995 and 2016 is  $-8.4^{\circ}\text{C}$  (Environment and Climate Change Canada, 2018). The mean annual air temperature in 2016 was  $-6.3^{\circ}\text{C}$ , which was higher in comparison to the reference period. The mean air temperatures for July ( $9.4^{\circ}\text{C}$ ) and August ( $7.7^{\circ}\text{C}$ ) in 2016 were also higher compared to the reference period ( $9.0$  and  $7.3^{\circ}\text{C}$ , respectively). Snowmelt occurs in late May or early June, when average monthly air temperatures are  $-3.4$  and  $4.2^{\circ}\text{C}$ , respectively (Burn, 2012). It is the largest hydrological event of the year (Coch et al., 2018). Freezeup of the active layer occurs commonly by mid-November (Burn, 2012).

The studied watersheds Water Creek, Beach Creek, Fox Creek, Ice Creek West (ICW), Ice Creek East (ICE), and Eastern Gully (unofficial names) are located on the eastern side of the island draining into the Beaufort Sea (Figure 1b). All rivers have similar characteristics in terms of elevation, slope, and aspect, but they vary in size (Table 1). Water Creek is the largest river with a catchment size of 2,678 ha, whereas Eastern Gully is the smallest with 44 ha in size. The paired watersheds ICW (138 ha) and East (165 ha) were sampled in more detail over the course of the season (Figure 1c). Both rivers merge before draining into an alluvial fan and finally into the sea. Ice-wedge polygons reach into the headwaters of ICW are visible in WorldView-3 2015 satellite images (Figure S1 in the supporting information).

### 3. Methods

#### 3.1. Mapping of Disturbances

The mapping was done in ArcGIS (ESRI, Version 10.3) using historical aerial photographs and high-resolution satellite images. The historical aerial photographs were taken in 1952 and 1970 with a black-and-white film and have a resolution of 3 and 0.8 m, respectively (National Air Photo Library, Canada). The GeoEye-1 and WorldView2 high-resolution satellite images (1.8 m in multispectral and 0.5 m in panchromatic view) were acquired on 31 August 2011 and 8 August 2015, respectively. The aerial photographs were orthorectified and georeferenced in PCI Geomatic's Geomatica Orthoengine© software (2014), based on the GeoEye-1 satellite images from 2011 (Irrgang et al., 2018).

Active disturbances were digitized in the six catchments at a 1:1,500 scale through manual interpretation. The disturbances include ALD and RTSs. Active RTSs are characterized by steep headwalls exposing ice-rich permafrost, slump floors with thawed sediments, and incised gullies. Active ALDs are characterized by a sharp scarp and a nonvegetated scar zone. Criteria used for manual interpretation and feature identification combined several characteristics described in Table S1. The available photographs from 1970 only cover ICW, ICE, and Eastern Gully, which is why the mapping in that year is constrained to those watersheds. Differences in spatial resolution between the aerial photographs and satellite images may impose further limitations in mapping accuracy. This difference was however deemed satisfactory for interpretation and mapping purposes (Ramage et al., 2017).

We used the SAGA toolbox (Version 2.3.2) in QGIS (Version 2.18.23) to delineate watersheds and channels based on a TerraSAR-X digital elevation model of 12-m resolution. QGIS was further used to determine which of the mapped disturbances are hydrologically connected, that is, intersect with the channels.

### 3.2. Stream Monitoring

The focus of this study is on the paired watersheds ICW and ICE (Figure 1c), where water quality and runoff were monitored over the summer monitoring season 25 July to 10 August 2016. Further, we collected water samples along longitudinal profiles and soil water samples along transects. The other rivers—Water Creek, Beach Creek, Fox Creek, and Eastern Gully—were only visited between 13 and 15 August in order to collect water samples and to measure runoff at the same time.

We installed a weather station at the outflow of ICW collecting air temperature (IST temperature sensor TSic 506;  $\pm 0.1$  °C accuracy) and precipitation (Young tipping bucket rain gauge 52203; accuracy  $\pm 2\%$ ) over the course of the monitoring season in 2016.

Discharge was recorded continuously in ICW and ICE between 25 July and 10 August. In ICW, a cutthroat flume ( $w = 0.2$  m,  $l = 0.7$  m, and  $h = 0.5$  m) was equipped with a U20 Onset Hobo level logger (U20-001-01;  $\pm 0.05\%$  accuracy) at a 5-min sampling interval. In order to compensate for the barometric pressure, another Hobo U20 level logger was secured with rebar close to the discharge station collecting barometric pressure at the same sampling interval. Discharge was computed based on a standard equation (Skogerboe et al., 1973) for the dimensions of the flume. In ICE, another U20 Hobo level logger was attached to a rebar and inserted into a flat cross section of the channel. Flow was measured manually 11 times using the portable Flo-Mate 2000 Flow Meter ( $\pm 2\%$  of reading) for four segments of the stream. A stage-discharge rating curve was established in order to retrieve discharge over the monitoring period. The area-velocity method was used to obtain discharge at the time of sample collection at ICW and ICE, Beach Creek, and Fox Creek on 13 August, at Eastern Gully on 14 August, and at Water Creek on 15 August. To compare runoff ratios between ICE and ICW, baseflow and event flow were separated using the subjective method (Singh, 1992). The runoff ratio for a rainfall event is obtained through dividing the runoff by the precipitation for the entire watershed.

Water samples were collected in ICW using an automatic water sampler (ISCO 3700) downstream of the flume. The sampling interval was set to 12 hr and increased during rainfall events (between 1 and 3 hr). Water sampling in ICE was done manually usually once per day. Between 13 and 15 August, manual samples were also collected at the outflow of the other rivers (Figure 1b). In addition to the sampling at the outflow of the rivers, samples were also taken along longitudinal profiles of the channels of ICW and ICE starting at the headwaters (Location 1) and following the river downstream (Location 12). This was done in ICW on 20, 25, and 30 July and in ICE on 30 July and 11 August. Thus, rainfall (20 July and 30 July) and postrainfall conditions (25 July and 11 August) were captured. For later analysis we subjectively assigned samples at location 1 to 5 to “upstream” and samples at location 6 to 12 to “downstream” (Figure 1c).

Piezometers—perforated PVC tubes of 100-cm length—were installed into the active layer along transects in the upper (profile P1), middle (profile P2), and lower (profile P3) catchment of ICW starting in the headwaters on 26 July (Figure 1c). A vacuum pump was used to collect soil water from the piezometers if water was available. Sampling took place on 29 and 30 July and 9 and 14 August. Ice screws were used to collect samples of intrasedimental ice for stable water isotope analyses after digging to the permafrost table.

Within 24 hr of sampling, electrical conductivity, pH, and turbidity were recorded in the field. Turbidity was measured with a LaMotte 2020wi portable turbidity meter ( $\pm 2\%$  accuracy for 2.5–100 FNU;  $\pm 3\%$  for >100 FNU) using blank, 10 and 100 FNU standards. For the Fox Creek sample, a 500 FNU standard was used. The majority of surface water samples were prepared for further hydrochemical analyses directly in the field, whereas the soil water samples were frozen immediately. Samples were analyzed for suspended sediment concentration (SSC; surface water), particulate organic carbon (POC; surface water), DOC (surface and soil water), total dissolved nitrogen (TDN; surface and soil water), dissolved ions (surface and soil water), and stable water isotopes (surface and soil water). In addition, deionized water used in the field was analyzed as blank following the same procedures described below. SSC and POC data are available from Coch et al. (2018).

SSC was obtained by volumetric vacuum filtration of samples through preweighed and precombusted 0.7- $\mu\text{m}$  glass fiber filters. They were dried at 50 °C for 24 hr and subsequently weighed. A maximum of 1,000 ml of sample water was filtered to obtain SSC. Out of the 133 surface water samples, 47 contained enough sediment with a minimum net weight of 10 mg. These 47 were milled using a mortar to homogenize the filter-sediment-mixture. Inorganic carbon was removed before duplicate measurements of 6 mg each were carried out in an elemental analyzer (Flash 2000, Thermo Scientific, Germany) to obtain  $C_{\text{org}}$  (%). This was also done for two blank filters to account for a possible signal from the filters. Based on the filtered volume and the net weights of filter and sample, POC concentrations in the suspended material (%) and POC concentrations in the water (mg/l) were determined.

Samples for DOC and TDN were acidified with HCl (30% suprapur) prior to the measurements. Analyses were performed on a Shimadzu TOC-L analyzer with a TNM-L module. Total inorganic carbon was sparged out with synthetic air prior to the measurement. There was a shortage of HCl in the field, which is why 82 samples collected between 29 July and 7 August were frozen in the field and acidified upon return. The period of different sample treatment is indicated in the data.

Samples were filtered through a cellulose acetate membrane syringe prefilter with a pore size of 0.45  $\mu\text{m}$  to prepare them for anion and cation measurements. To conserve cation subsamples, 65%  $\text{HNO}_3$  (Suprapur) was used. Due to the lack of acid, 82 cation subsamples were frozen and conserved upon return to the laboratory. Dissolved cations  $\text{Al}^+$ ,  $\text{Ba}^{2+}$ ,  $\text{Fe}$ ,  $\text{Mn}$ ,  $\text{Sr}^{2+}$  (in  $\mu\text{g l}^{-1}$ ),  $\text{Ca}^{2+}$ ,  $\text{K}^+$ ,  $\text{Mg}^{2+}$ ,  $\text{Na}^+$ ,  $\text{P}$ , and  $\text{Si}^{4+}$  (in mg/l) were determined on a Perkin Elmer Optima3000XL ICP-OES spectrometer. A Dionex DX-320 ion chromatograph was used to measure dissolved anions  $\text{F}^-$ ,  $\text{Cl}^-$ ,  $\text{SO}_4^{2-}$ ,  $\text{Br}^-$ ,  $\text{NO}_3^-$ , and  $\text{PO}_4^{3-}$  (in mg/l). Measurements of  $\text{HCO}_3^-$  (mg/l) concentrations were performed on a Metrohm Titrino 794 titrator. Total dissolved solids (TDS) reported in this study are the sum of all dissolved anions and cations. For data processing and statistical analysis, concentrations below detection limit were set to the detection limit. The charge balance error was computed following Freeze and Cherry (1979), resulting in a mean of 0.57% and remaining below 10.4% for all surface and soil water samples. Sulfate is known to increase in disturbed areas (Abbott et al., 2015; Kokelj et al., 2005; Kokelj et al., 2013). Thus, we chose to examine TDS and sulfate in detail in this study. The complete hydrochemical data set will be available through PANGAEA.

Samples for stable water isotopes,  $\delta\text{D}$  and  $\delta^{18}\text{O}$ , were stored in vials with airtight caps. The samples were measured on a Finnigan MAT Delta-S mass spectrometer equipped with two equilibration units for the online determination of hydrogen and oxygen isotopic composition (Meyer et al., 2000). The external errors are lower than 0.8‰ for hydrogen and below 0.10‰ for oxygen. The second-order parameter  $d$  excess is calculated ( $d$  excess =  $\delta\text{D} - 8 \cdot \delta^{18}\text{O}$ ; Dansgaard, 1964) and indicative for nonequilibrium fractionation processes.

### 3.3. Flux Estimates and Statistics

To determine flux estimates for a parameter ( $F_p$ ), mean runoff volume  $\bar{Q}$  during every time step  $t$  was multiplied with the concentration of the parameter  $[P]_t$  at that time. The flux estimates are summed for the time interval of interest  $t_n$  (equation (1)).

$$F_p = \sum_{t_0}^{t_n} (\bar{Q} \times [P]_t) \quad (1)$$

The mean runoff volume  $\bar{Q}$  for a time interval of interest  $t_n$  is the mean of all discharge runoff values from half the interval before and after  $t_n$  (equation (2)). For example, if the interval is 6 hr, the mean is computed from 3 to 9 hr. Flux estimates are reported in kg per mm of runoff (kg/mm).

$$\bar{Q} = n^{-1} \sum_{t_0 - \frac{t_n}{2}}^{t_n + \frac{t_n}{2}} Q_t \quad (2)$$

Statistical tests in this study were performed using RStudio (Version 1.0.153). Normality of distributions were tested by applying the Shapiro-Wilk normality test.

To compare the means of two populations, in this case, for example, DOC concentrations at the outflow of the neighboring watersheds ICW and ICE, the Welch's two sample  $t$  test was used for normally distributed

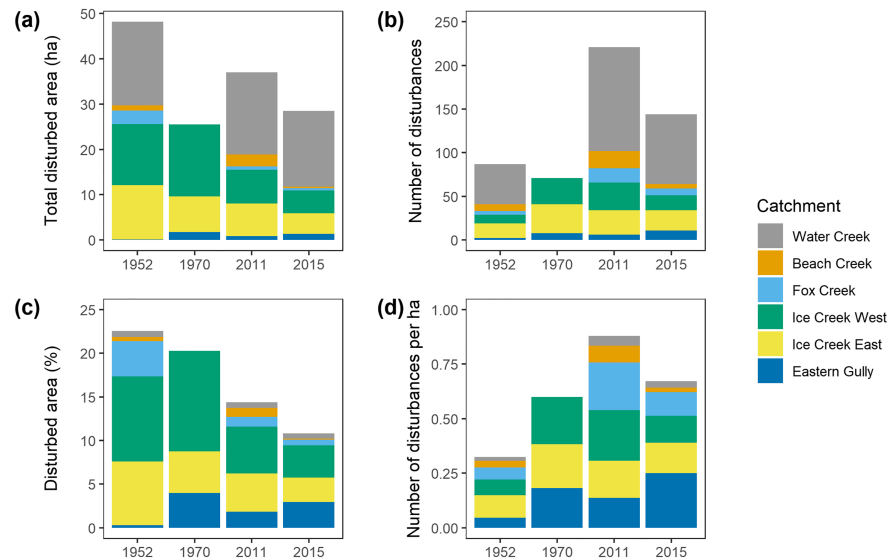


**Figure 2.** Mapping of disturbances in 1952 (aerial photograph), 1970 (aerial photograph), 2011 (Geo-Eye satellite image), and 2015 (WorldView-3 satellite image) showing (a) total disturbed area in ha, (b) total number of disturbances, (c) relative disturbed area in %, and (d) number of disturbances per hectare for the catchments Water Creek, Beach Creek, Fox Creek, Ice Creek West, Ice Creek East, and Eastern Gully (west to east). Note that the 1970 aerial photograph only covered Ice Creek West, Ice Creek East, and Eastern Gully.

data with unequal variances. If data were not normally distributed, the Wilcoxon-Mann-Whitney test was used. To measure the relationship between two variables, the Pearson correlation coefficient was applied.

## 4. Results

### 4.1. Catchment Disturbance

Active disturbances were found in all studied watersheds between 1952 and 2015 (Figures 2 and S2). The total disturbed area for all watersheds decreased by 41% between 1952 and 2015 (Figure 2a), whereas the total number of disturbances increased by 66% (Figure 2b). The highest total number of disturbances occurred in 2011 (221). We found a gradual decrease of disturbed area cumulative for all watersheds between 1952 and 2015 (Figure 2c). The relative number of disturbances peaked in 2011 and decreased in 2015 (Figure 2d).

Relative to their size, the mean disturbed area for all watersheds over 1952, 2011, and 2015 was  $2.7 \pm 1.2\%$ . ICW and ICE had the greatest mean disturbed area over these years ( $6.3 \pm 2.6\%$  and  $4.8 \pm 1.9\%$ , respectively). Beach Creek had the least disturbed area  $0.5 \pm 0.4\%$  over the same period. The number of disturbances per hectare was on average  $0.10 \pm 0.05$ . ICW, ICE, and Eastern Gully had the highest relative number of disturbances over 1952, 2011, and 2015 ( $0.14 \pm 0.07$ ,  $0.14 \pm 0.03$ , and  $0.14 \pm 0.08$ ).

### 4.2. Runoff and Hydrochemistry

During the time of stream monitoring of ICW and ICE, two rainfall events of 9.3 and 12.7 mm were recorded (Figure 3a). Prior to stream monitoring, an event of 33.9 mm occurred (Coch et al., 2018). Runoff in both watersheds followed rainfall events. Peakflow during the time of monitoring reached  $0.011 \text{ m}^3/\text{s}$  in ICW and  $0.012 \text{ m}^3/\text{s}$  in ICE. The watersheds responded quickly to rainfall events, as shown by the linear rising hydrographs and the quick return to baseflow conditions thereafter (Figure 3a). Rainfall-to-runoff ratios were in a similar range 0.14 and 0.13 in ICW, 0.15 for both events in ICE (Table 2). In both rivers, baseflow increased after each rainfall event.

DOC concentrations were  $7.6 \pm 1.4 \text{ mg/l}$  in ICW and in  $7.2 \pm 1.5 \text{ mg/l}$  in ICE. There was no significant difference between both creeks (Table 3). The DOC flux over the monitoring period was  $10.5 \text{ kg/mm}$  for ICW and  $11.8 \text{ kg/mm}$  for ICE.

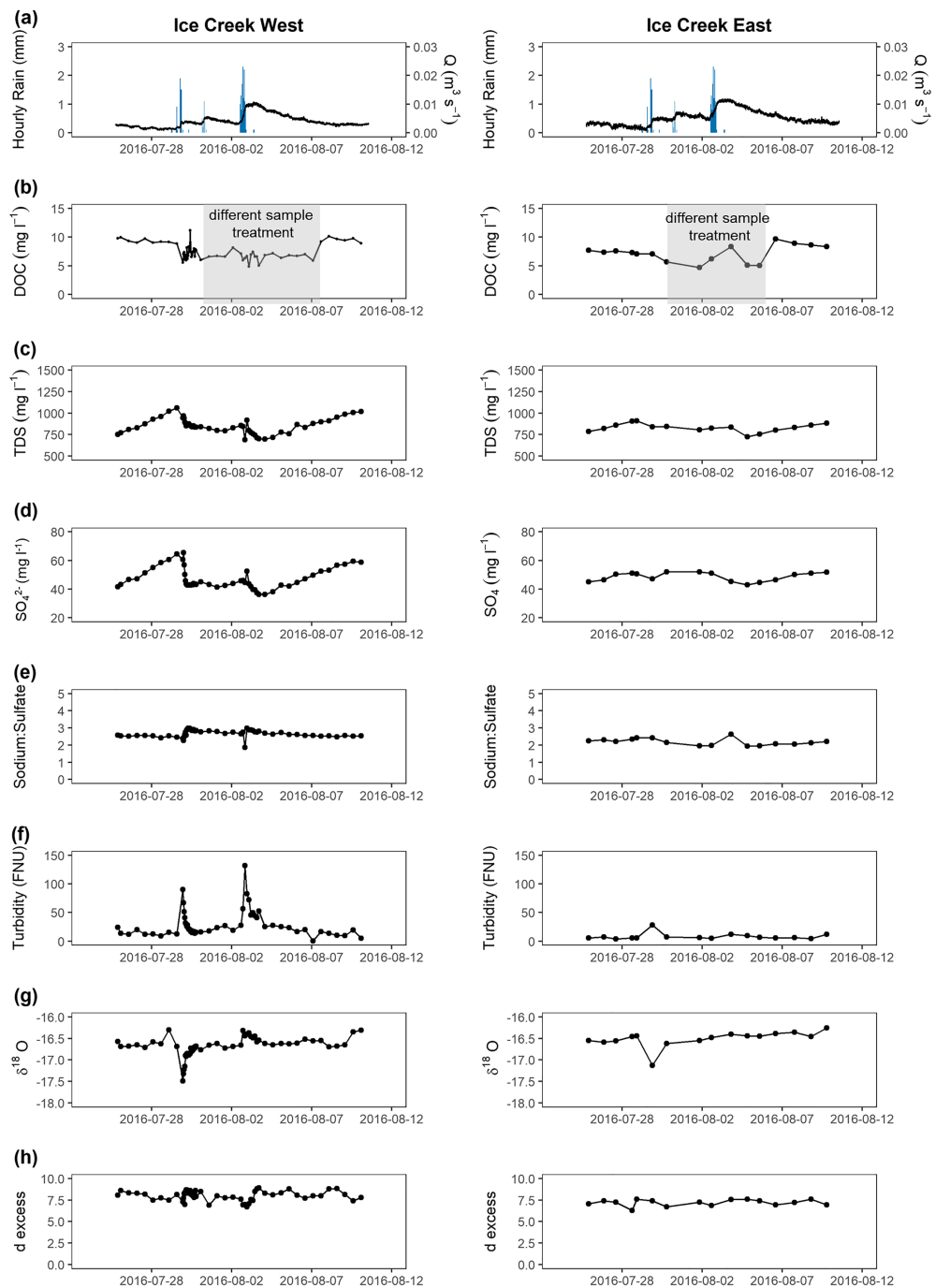


**Figure 3.** Rainfall, hydrographs, and hydrochemistry data from Ice Creek West and Ice Creek East during the summer monitoring season of 2016. (a) Hourly rainfall and discharge, (b) DOC, (c) TDS, (d)  $\text{SO}_4^{2-}$ , (e) Na: $\text{SO}_4$ , (f) turbidity, (g)  $\delta^{18}\text{O}$ , and (h) deuterium excess (d excess). Note that differences in sample treatment for DOC samples are indicated in gray.

Concentrations of TDS in ICW ( $853 \pm 84$  mg/l) and ICE ( $831 \pm 51$  mg/l) were not significantly different from each other. The total TDS flux amounted to 1,140 kg/mm for ICW and to 1,350 kg/mm for ICE. We found a decrease in TDS and  $\text{SO}_4^{2-}$  concentration with increasing runoff in both watersheds. The major ions contributing to the sum of TDS in both watersheds were (highest to lowest)  $\text{HCO}_3^-$ ,  $\text{Cl}^-$ ,  $\text{Na}^+$ ,  $\text{Ca}^{2+}$ ,  $\text{SO}_4^{2-}$ , and  $\text{Mg}^{2+}$ . The ratio of Na: $\text{SO}_4$  differed significantly ( $p < 0.05$ ) at the outflow of both creeks,  $2.7 \pm 0.2$  for ICW and  $2.2 \pm 0.2$  for ICE (Tables 3 and S2; Figure 3d).

**Table 2**

Fluxes of DOC, TDN, TDS, and SS Between 25 July and 10 August 2016 and the Runoff Ratios for Both Rainfall Events on 29–31 July (9.3 mm) and 2–3 August (12.7 mm)

	Ice Creek West (ICW)	Ice Creek East (ICE)
DOC (kg/mm)	10.5	11.8
TDN (kg/mm)	0.7	0.6
TDS (kg/mm)	1,140	1,350
SS (kg/mm)	32.8	12.1
Runoff ratio 1 (9.3 mm)	0.14	0.15
Runoff ratio 2 (12.7 mm)	0.13	0.15

Note. The flux calculation is based on the same time steps for ICW and ICE. Due to the lower sampling frequency in ICE and missing data on 30 July, the sampling frequency of ICW was adjusted accordingly.

We further found a significant difference in turbidity between both rivers. Turbidity (Figure 3f) in ICW was significantly ( $p < 0.05$ ) higher ( $28.3 \pm 23.3$  FNU) than in ICE ( $8.2 \pm 5.9$  FNU). The temporal pattern followed rainfall events; an increase in turbidity was related to an increase in runoff. We compared turbidity values with SSC and found a strong positive linear relationship ( $R^2 = 0.91$ ,  $p < 0.05$ ). By using the regression formula ( $SSC = 0.94 * \text{turbidity} + 0.26$ ), SSC can be determined (Figure S3). Based on the measured SSC values, we found a SS flux of 32.8 kg/mm in ICW and 12.1 kg/mm in ICE. There is also a strong positive linear relationship between SSC and POC ( $R^2 = 0.97$ ,  $p < 0.05$ ), which allows to extrapolate from SSC to POC ( $POC = 0.02 * SSC + 0.05$ ; Figure S4). Around 2% of suspended sediment is composed of POC. Full details and discussion of SSC and POC were given in a previous study by Coch et al. (2018).

The isotopic signature (deuterium excess) shows a small but significant difference ( $p < 0.05$ ) between both creeks ( $8.0 \pm 0.6$  for ICW;  $7.2 \pm 0.4$  for ICE). Values of  $\delta^{18}\text{O}$  and  $\delta\text{D}$  amount to  $-16.7 \pm 0.2\text{‰}$  and to  $-125.5 \pm 1.8\text{‰}$  in ICW and to  $-16.5 \pm 0.2\text{‰}$  and to  $-124.9 \pm 1.5\text{‰}$  in ICE. They follow a similar pattern over the course of the season in both streams. After the first rainfall event,  $\delta^{18}\text{O}$  dropped to  $-17.5\text{‰}$  in ICW and to  $-17.1\text{‰}$  in ICE accompanied with an increase in the d-excess value. The second rainfall event leads to an increase in  $\delta^{18}\text{O}$  to  $-16.4\text{‰}$  accompanied with a decrease in the d-excess. This peak is not detected in ICE.

The relationship between  $\delta^{18}\text{O}$  and  $\delta\text{D}$  is depicted in Figure 5. The correlation based on all samples collected follows the equation  $\delta\text{D} = 6.4 \delta^{18}\text{O} - 17.9$  ( $R^2 = 0.94$ ,  $p < 0.05$ ). The slope is lower than that of the nearest local meteoric water line at Inuvik ( $\delta\text{D} = 7.3 * \delta^{18}\text{O} - 3.6$ ,  $R^2 = 0.98$ ; IAEA/WMO, 2018). Values for  $\delta^{18}\text{O}$ ,  $\delta\text{D}$ , and deuterium excess yield  $-16.7 \pm 0.2\text{‰}$ ,  $-125.5 \pm 1.8\text{‰}$ , and  $8.0 \pm 0.6\text{‰}$  in ICW and  $-16.5 \pm 0.2\text{‰}$ ,  $-124.9 \pm 1.5\text{‰}$ , and  $8.3 \pm 1.5\text{‰}$  in ICE, respectively. Precipitation shows a high variability becoming more enriched over the course of the season. Mean values of  $\delta^{18}\text{O}$ ,  $\delta\text{D}$ , and deuterium excess for precipitation, ICW intra-sedimental ice, and ICW soil water are given in Table 4. The isotope composition from headwaters to downstream is presented in section 4.3.

### 4.3. Lateral Transport of Stream Water

Water quality changes along the longitudinal stream profiles are presented in relation to recent disturbances (Figure 5a). They were found across both watersheds in 2015, but their number and aerial distribution varied between the streams (Figure 5a). In 2015, the total number of disturbances was 17 in ICW and 23 in ICE, and the relative disturbed area was 3.7% and 3.1%, respectively. The highest number of disturbances was found downstream in ICE (21), followed by the headwaters of ICW (11). The headwaters of ICW showed the highest relative disturbed area in 2015 (3.0%), followed by downstream ICE (2.3%). Overall, it seemed that recent disturbances occurred throughout the upstream and downstream catchments of ICW, whereas especially,

**Table 3**

Results of Statistical Tests of Equal Means (Welch's Two Sample *t* Test for Normally Distributed Data; Wilcoxon-Mann-Whitney Test for Not Normally Distributed Data) for Measured Parameters

	ICE vs. ICW outflow	ICE upstream vs. ICE downstream	ICW upstream vs. ICW downstream	ICE upstream vs. ICW upstream	ICE downstream vs. ICW downstream
DOC	$p > 0.05$	$p > 0.05$	$p < 0.05$	$p < 0.05$	$p < 0.05$
TDS	$p > 0.05$	$p > 0.05$	$p < 0.05$	$p < 0.05$	$p < 0.05$
Na:SO <sub>4</sub>	$p < 0.05$	$p < 0.05$	$p < 0.05$	$p < 0.05$	$p < 0.05$
SO <sub>4</sub> <sup>2-</sup>	$p < 0.05$	$p < 0.05$	$p < 0.05$	$p < 0.05$	$p < 0.05$
Turbidity	$p < 0.05$	$p < 0.05$	$p < 0.05$	$p < 0.05$	$p < 0.05$
$\delta^{18}\text{O}$	$p < 0.05$	$p > 0.05$	$p > 0.05$	$p > 0.05$	$p < 0.05$
d-excess	$p < 0.05$	$p > 0.05$	$p > 0.05$	$p > 0.05$	$p < 0.05$

Note. We compared ICW and ICE and the respective upstream and downstream locations. Upstream comprises sampling Locations 1–5, Downstream 6–12.  $p < 0.05$  indicates a significant difference between the means of the parameters.

**Table 4**  
Mean  $\delta^{18}\text{O}$ ,  $\delta\text{D}$ , and Deuterium Excess Values for Samples of Precipitation, ICW Intrasedimental Ice, and ICW Soil Water

	$\delta^{18}\text{O}$ (‰)	$\delta\text{D}$ (‰)	Deuterium excess (‰)	<i>n</i>
Precipitation	$-15.5 \pm 3.2$	$-121.3 \pm 21.9$	$2.6 \pm 4.2$	4
ICW intrasedimental ice	$-17.8 \pm 0.5$	$-134.3 \pm 4.8$	$7.8 \pm 1.1$	5
ICW soil water	$-16.8 \pm 0.8$	$-126.2 \pm 4.9$	$8.3 \pm 1.5$	34

Note. See Table S4 for isotope values of different locations.

the downstream catchment of ICE is impacted. The landscape had been stronger impacted by disturbances in the past (Figure S2), with higher number and more relative disturbed areas downstream in ICW and ICE.

The hydrochemical patterns differed between both watersheds (Figures 5b and 5c; Table 3). Concentrations of DOC were significantly higher ( $p < 0.05$ ) in ICW, where degrading ice-wedge polygons impact the headwaters. DOC decreased after the first rainfall event (20 July) at all locations in ICW. On the contrary, DOC concentrations in ICE remained on the same level with a slight decrease from headwaters to downstream. On 30 July, when both creeks were sampled simultaneously, downstream concentrations were in a similar range, ICW showing slightly lower values ( $7.3 \pm 0.8$  mg/l) than ICE ( $8.0 \pm 0.2$  mg/l).

The TDS pattern along the longitudinal profile also differed significantly between both creeks (Figure 5b). TDS was significantly lower ( $p < 0.05$ ) in the headwaters and downstream in ICW than in ICE. On 30 July, headwater TDS concentration in ICW was  $489 \pm 220$  mg/l and  $934 \pm 140$  mg/l in ICE. Downstream TDS concentrations were  $741 \pm 64$  mg/l in ICW and  $873 \pm 19$  mg/l in ICE. A slight increase in TDS was visible over the course of the season.

Both  $\text{SO}_4^{2-}$  and Na: $\text{SO}_4$  patterns differed strongly between the creeks (Figures 5c and 5d). A downstream increase of  $\text{SO}_4^{2-}$  (decrease of Na: $\text{SO}_4$ ) occurs with a recent hydrologically connected disturbance at Location 9 in ICW. At Location 1 in ICW, Na: $\text{SO}_4$  is exceptionally high through a domination of calcium and bicarbonate and very low levels in sulfate.  $\text{SO}_4^{2-}$  concentrations throughout ICE are significantly higher ( $p < 0.05$ ) than in ICW. Location 1 is directly impacted by a hydrologically connected disturbance.

We found a general increase in turbidity from upstream to downstream in ICW and ICE. This difference was significant ( $p < 0.05$ ) in both streams. In ICW, turbidity peaked at Location 7 on 25 July (postrain conditions), which amounted to 48.7 FNU and dropped thereafter. At this location, we could not identify any hydrologically connected disturbances. During the subsequent rainfall event on 30 July, there was no peak at the same location anymore (9.3 FNU). Compared to ICE, downstream turbidity values were significantly higher ( $p < 0.05$ ) in ICW. ICE showed similar patterns during 30 July and 11 August. There was an increase in turbidity from Location 6 onward, showing a peak at Location 8. During rainfall conditions, this peak amounted to 14.9 FNU and declined gradually toward the outflow of the river. During postrain conditions, on 11 August, turbidity peaked at the same location (11.2 FNU). This location was located directly after the inflow of a heavily disturbed water tributary (Figure 5a).

The stable isotope signatures of water were variable upstream and downstream within both creeks. These changes, however, were not statistically significant. We found that the values in  $\delta^{18}\text{O}$  and  $\delta\text{D}$  corresponded well with each other in both creeks (Figure 4).

Section 4.2 described  $\delta^{18}\text{O}$  and  $\delta\text{D}$  values for precipitation and intrasedimental ice and the local meteoric water line. Location 1 in ICW showed the lowest  $\delta^{18}\text{O}$  (closer to the intrasedimental ice signal) compared to the locations further downstream, which showed higher values. In contrast, ICE shows the opposite trend with higher  $\delta^{18}\text{O}$  values upstream than downstream. The d-excess pattern follows a contrary behavior in both streams. On 30 July, the  $\delta^{18}\text{O}$  values in ICW and ICE were similar to each other, whereas d-excess was higher in ICW ( $8.4 \pm 1.0$ ‰) than in ICE ( $6.5 \pm 0.7$ ‰).

#### 4.4. Hydrochemical Composition and Fluxes in Nearby Streams

There were strong positive relationships ( $p < 0.05$ ) between daily DOC, TDN, and TDS fluxes and total catchment area for all rivers (Figure 6). The lowest daily fluxes were recorded in Eastern Gully, and the highest ones in Water Creek. This relationship remained significant ( $p < 0.05$ ) also when excluding the largest

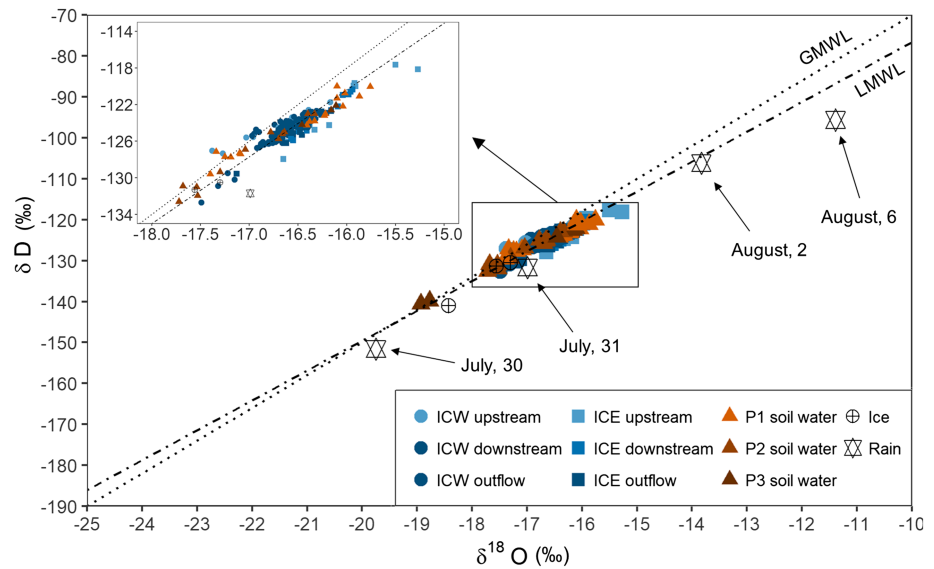


**Figure 4.** Co-isotope relation between  $\delta^{18}\text{O}$  (‰) and  $\delta\text{D}$  (‰) for river water, ICW soil water, and ICW intrasedimental ice and rainwater. The blue color gradient indicates samples from upstream (Locations 1–5), downstream (Locations 6–11), and the outflow of Ice Creek West (ICW) and Ice Creek East (ICE). The orange color gradient reflects soil water samples extracted from the piezometer profiles from the upper catchment (P1) to the lower catchment (P3) in ICW. The lines represent the Global Meteoric Water Line (GMWL)  $\delta\text{D} = 8 \delta^{18}\text{O} + 10$  by Craig (1961) and the local meteoric water line (LMWL)  $\delta\text{D} = 7.3 \delta^{18}\text{O} - 3.6$  by IAEA/WMO (2018).

catchment (Water Creek) from the regression (Figure S5; Table S3). The slopes of the regression lines including and excluding Water Creek were not statistically different (one-way ANCOVA  $F$  statistic,  $p > 0.05$ ). There was a strong positive relationship between daily SS flux and total catchment area if we excluded Fox Creek. In Fox Creek, there was a RTS, which was visible in the 2011 imagery and which mobilized substantial amounts of sediment. The total sediment flux for Fox Creek amounted to  $402 \text{ kg}\cdot\text{mm}^{-1}\cdot\text{day}^{-1}$ . Fox Creek shows a  $\delta^{18}\text{O}$  of  $-17.1\text{‰}$ , which is above the average of all streams on that day ( $-16.6 \pm 0.3\text{‰}$ ) and closer to the intrasedimental ice signal. No significant relationships between relative disturbed area (%) nor relative number of disturbance and hydrochemical fluxes were found. At this point in the season, at postrain conditions, hydrochemical fluxes seemed to be controlled by catchment size.

## 5. Discussion

### 5.1. Total Runoff and Water Quality

The hydrological response of the adjacent watersheds ICW and ICE is similar. Summer baseflow seems to be controlled by rainfall events in both creeks. The runoff ratios ICW and ICE are in the same order of magnitude ( $0.14 \pm 0.0$  and  $0.15 \pm 0.0$ , respectively), suggesting inefficient water routing and a high storage capacity in the catchments. This finding corresponds with runoff ratios reported from ICW by Coch et al. (2018) over the summers 2014, 2015, and 2016. Based on complete data of six rainfall events, they estimated a runoff ratio in ICW of  $0.11 \pm 0.02$ . Runoff ratios are also reported from other locations across the Arctic. Carey et al. (2013) measured runoff ratios between 0.29 and 0.66 in a  $7.6\text{-km}^2$  alpine headwater stream (Granger Basin), which is located in the discontinuous permafrost zone. Conditions in the catchment prior to rainfall events were more saturated in order to route water more efficiently. Favaro and Lamoureux (2014) reported a high variability of rainfall-runoff ratios between 0.001 and 0.84 in an  $8.0\text{-km}^2$  watershed (West River) at Cape Bounty, Melville Island, in the High Arctic. They also found the antecedent soil moisture conditions an important factor controlling the water routing. Future increase in summer precipitation across the Arctic (Bintanja & Andry, 2017) could lead to higher summer runoff and therefore higher runoff ratios.

The total export of DOC, TDN, and TDS is in the same order of magnitude throughout the course of the monitoring season. Taking the surrounding rivers into account indicates a proportionate increase of the output of these parameters with catchment size (Figure 6). This, however, does not apply for the output of suspended

sediment. We find that ICW exports more than twice the amount of sediment (32.8 kg/mm) than ICE (12.1 kg/mm). This shows the variability of sediment export across catchments over time. Coch et al. (2018) examined sediment outputs from ICW in relation to rainfall events in 2015 and 2016. They found a strong variability between both seasons and explain that there is an overall limitation of sediment supply within the river. Interannual variability was presumably caused by localized disturbances and riverbank erosion.

There are potential limitations to using the relationship of catchment size and hydrochemical output per mm for upscaling exercises. To strengthen this empirical relationship, more catchments covering a range of sizes need to be studied over time within the same ecoregion. Another challenge is the lack of runoff data, which puts another constraint to upscale unmonitored rivers. Further, our data only provide insights into catchment processes during the summer. Snowmelt is the largest hydrological event of the year (M. Woo, 2012) and responsible for major matter export from Arctic rivers (Fouché et al., 2017; Lamoureux & Lafrenière, 2018; Laudon et al., 2004; Petrone et al., 2006). Incorporating all seasons into the water balance and hydrochemical export studies is essential to assess lateral fluxes into the ocean.

## 5.2. Water Quality Changes From Headwaters to Downstream

Concentrations measured at the outflow of a stream are an integrator of all processes occurring in a catchment. We find that the water quality is changing between headwaters towards the outlet of the stream. Based on the proximity and similar hydrological response of both studied creeks, one could expect similar water quality changes between headwaters and downstream. However, the behavior differs, suggesting different processes dominating each creek. In ICW there is a significant difference of DOC, TDS,  $\text{SO}_4^{2-}$ ,  $\text{Na}:\text{SO}_4$ , and turbidity between headwaters and downstream. In contrast, ICE only shows significant differences in turbidity,  $\text{SO}_4^{2-}$ , and  $\text{Na}:\text{SO}_4$  between upstream and downstream.

We find a strong difference in DOC along the longitudinal profiles of ICW and ICE, despite similar soil organic carbon values in the streams (Eischeid, 2015). ICW shows significantly higher DOC concentrations upstream than downstream. Locations 1 and 4 have a rise in DOC concentrations. A careful visual examination of the 2011 and 2015 satellite images reveals the presence of high centered ice-wedge polygons in the upstream catchments, especially in ICW (Figure S1). The tributary stream catchment in ICW entering the mainstream just before Location 4 is also characterized by ice wedge polygons. ICE does not show a significant difference in DOC between upstream and downstream. Kokelj et al. (2014) investigated the distribution of ice wedge polygons east of the Mackenzie Delta, NWT, and revealed a surface coverage of up to 40% in the northernmost dwarf-shrub tundra—the same ecoregion as our study site. Liljedahl et al. (2016) highlighted the importance of ice-wedge degradation for the landscape's water balance. They observed a succession of degrading ice wedges across the Arctic and increased drainage over time. Increased drainage as a consequence of degrading ice wedges had been found to increase DOC loss in Yedoma permafrost regions (Vonk et al., 2013). We assume that the high DOC concentrations upstream in ICW may be connected to the degradation of ice-wedge polygons there. This is also indicated by the stable water isotopes values, showing significantly ( $<0.05$ ) lower values in the headwaters than downstream in ICW. The signal there is closer to the intrasedimental ice signal. The DOC concentration of ice wedges on Herschel Island has been determined to be  $8.3 \pm 4.4$  mg/l (Tanski et al., 2016). Further, ice-wedge polygon degradation creates an enhanced trough-channel network, thus forming riparian zones with high soil moisture. This increases the productivity of vegetation (Schuur et al., 2007) providing fresh DOC to be mobilized during rainfall events. We therefore assume that the DOC originates from near the surface (i.e., vegetation and organic material in the active layer) that is leached through increased drainage as well as the thawing permafrost. Runoff plays an important role in mobilizing DOC as found by Coch et al. (2019). They saw a proportionate increase of DOC export with runoff volume. DOC sources in ICW are widely available throughout the watershed. We conclude that downstream DOC concentrations are only reflecting the upstream conditions in ICE. In ICW, ice-wedge polygon degradation possibly causes increased DOC concentrations upstream, which are not reflected downstream. This indicates dilution or degradation processes of DOC downstream. Coch et al. (2019) examine the lateral transformation of DOC along the streams and confirm the assumption of degradation processes of the bioavailable DOC.

Stream water enrichment of TDS and  $\text{SO}_4^{2-}$  in particular is associated with runoff through disturbed areas (Abbott et al., 2015; Kokelj et al., 2005; Kokelj et al., 2013; Zolkos et al., 2018). In ICW, concentrations of TDS and  $\text{SO}_4^{2-}$  are increasing gradually along the longitudinal profile to the outflow. The hydrologically

connected disturbance at Location 9 directly increases  $\text{SO}_4^{2-}$  concentrations in ICW. The significantly higher  $\text{SO}_4^{2-}$  and lower  $\text{Na}:\text{SO}_4$  throughout ICE suggests that disturbances have had a stronger fluvial impact here. At Location 1, a hydrologically connected disturbance directly at the stream results in  $\text{SO}_4^{2-}$  concentrations of about 250 mg/l on 11 August. Lafrenière and Lamoureux (2013) studied disturbed catchments at Cape Bounty, Melville Island, in the High Arctic and found that impacts of disturbances on solute fluxes become evident with a higher degree of hydrological connectivity. We find that disturbances directly connected to the main channel influence  $\text{SO}_4^{2-}$  concentrations.

An increase in suspended sediment downstream is found in rivers where channel erosion processes are dominant (Dedkov, 2004). This is explained by the increase in discharge, thus the ability to mobilize more material. Disturbances, such as ALDs, act as local sediment sources when they are hydrologically connected to the stream (Favaro & Lamoureux, 2015). In ICW, we detect a peak in turbidity at Location 7 on 25 July, which is, however, not there anymore during the following rainfall event on 30 July. This suggests that the sediment source at this location was short-lived and rapidly exhausted. Despite the increase in discharge during the subsequent rainfall event, no sediment was available anymore that could have been mobilized. The sudden drop after the peak indicates that sediment is dispersed and deposited quickly. A sudden decrease in turbidity is also visible in ICE after the peak at Location 8, which points toward similar processes of mobilization and deposition. However, this location seems to be a constant source of sediment as the peak is visible during rainfall (30 July) and postrainfall (11 August) conditions. The likely source here is a disturbed and hydrologically connected gully (Figure 5a), which delivers sediment throughout the monitoring season. Turbidity as a proxy of SSC at the outflow of a stream reflects a source in close proximity and not necessarily the overall conditions of the entire stream. This finding is supported by Coch et al. (2018), who assess discharge sediment relationships for several rainfall events of different magnitudes for ICW between 2015 and 2016. Their data suggest a close proximity of local sediment sources and a rapid exhaustion.

### 5.3. Changes in Hydrochemistry and Isotopic Composition Over Time

The hydrochemical composition over the summer is closely related to rainfall events. The rainfall event occurring before 20 July led to the highest DOC concentrations in ICW. The levels had dropped 5 days after this event but remain still higher than after the following rainfall event (9.3 mm) on 30 July. TDS concentrations are lower on 20 July, reflecting the dilution effect through rainfall. The levels rise thereafter, remaining in a similar range in ICW on 25 and 30 July, and in ICE on 30 July and 11 August. Changes in turbidity are also linked to rainfall events, with a general increase as runoff increases. However, local short-lived sediment sources near the channel may occur and lead to localized increases. Our sampling reflects middle to late summer conditions in the catchments.

Generally, the water stable isotope signatures reflect the soil water conditions in the catchment. At the outflow of both streams (Figure 3) changes in water source over the season are visible. The first recorded rainfall event leads to a drop of stable water isotope values accompanied by an increase in  $d$ -excess. Fritz et al. (2011) found that  $\delta^{18}\text{O}$  of massive ground ice on Herschel island ranges between  $-39\text{‰}$  and  $-21\text{‰}$ , which is lower than our intrasedimental ice sample at the bottom of the active layer. Conversely, the second rainfall event results in an increase of stable water isotope values and a decrease in  $d$ -excess in ICW. Suprapermafrost water influenced by the underlying permafrost and possibly snowmelt was forced out (pistonning effect) and contributed to runoff during the first rainfall event. The runoff of the second rainfall event reflects the isotopic signature of rain. It may not have been captured in ICE due to the low sampling interval there. The changes in stable water isotopes along the longitudinal stream profiles confirm this effect. The very low runoff ratios of  $0.14 \pm 0.0$  for ICW and  $0.15 \pm 0.0$  for ICE show the high storage capacity of the catchments. Subsurface flow is important to mobilize solutes from the active layer as also found by Coch et al. (2018). Isotopic composition along a longitudinal profile had also been measured in West River on Cape Bounty, Melville Island, in the High Arctic by Bolduc et al. (2018). They also find an increase of stable isotopes through rainfall, and progressively downstream from the headwaters.

Different water sources are apparent along the longitudinal stream profiles. The headwaters in ICW show lower stable water isotope values than downstream. As discussed previously, this is most likely linked to the degrading ice-wedge polygons—a version of permafrost degradation. Mixing of surface water occurs on the way downstream. In contrast, ICE does not seem to have varying water sources along the stream profile. Further, none of the mapped disturbances alter the isotopic composition of the streams.

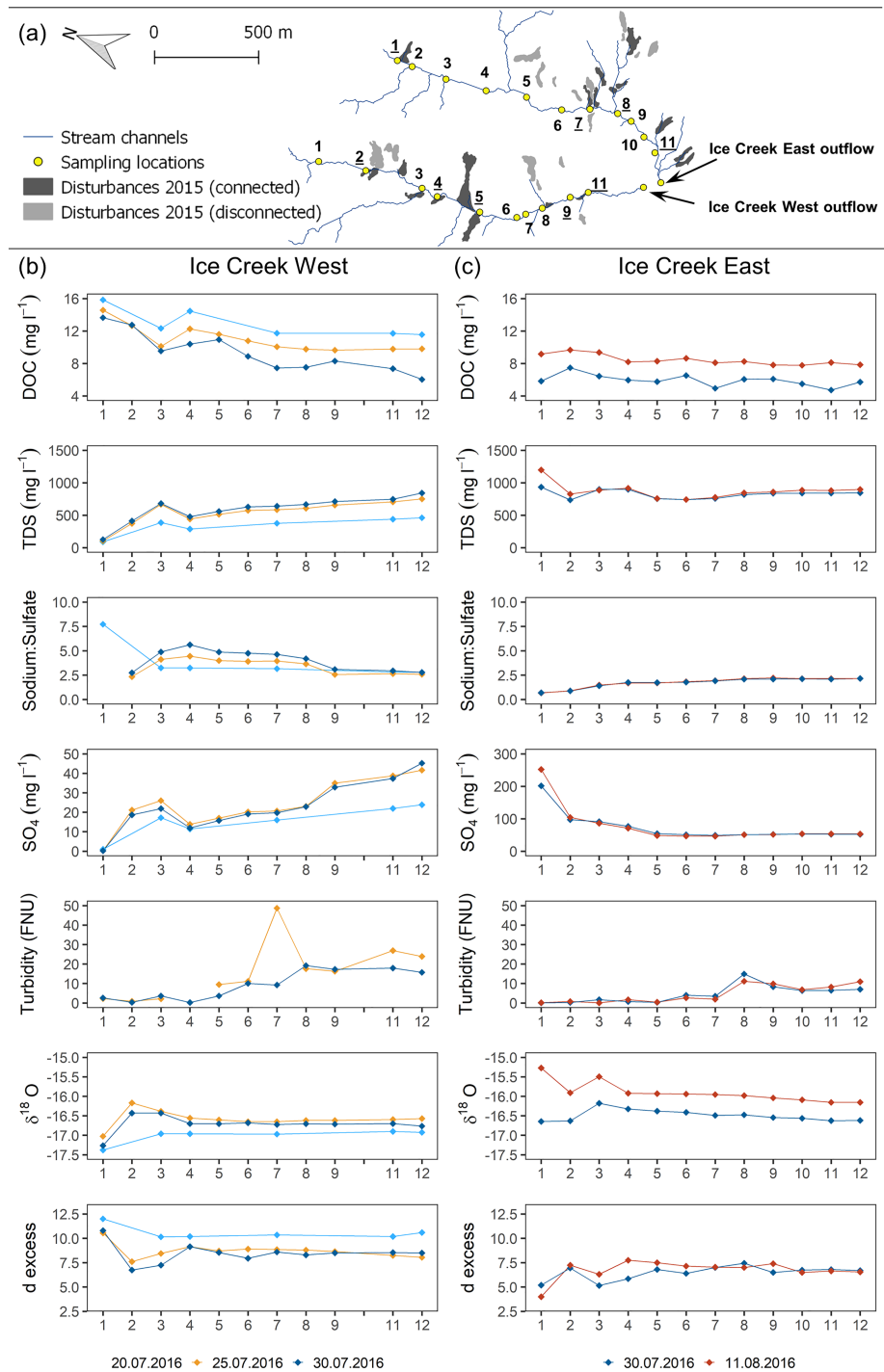


**Figure 5.** (a) Map of water sampling transects from headwater (Location 1) to downstream (Location 12) including recent (2015) disturbances (gray). The dark gray indicates a hydrological connection to the stream, impacting individual sampling locations (underlined). Results of DOC, TDS, SO<sub>4</sub><sup>2-</sup> (notice the scale change here between ICW and ICW), Na:SO<sub>4</sub>, turbidity, δ<sup>18</sup>O, and d-excess are presented for each location of (a) Ice Creek West and (b) Ice Creek East. Blue colors indicate rainfall events, yellow/red postrain conditions. Due to technical problems, there is no data for sampling point “10” in ICW and no turbidity data on 20 July. Note that the scale for Na:SO<sub>4</sub> excludes outliers at Location 1 in ICW to capture the variability along the stream.

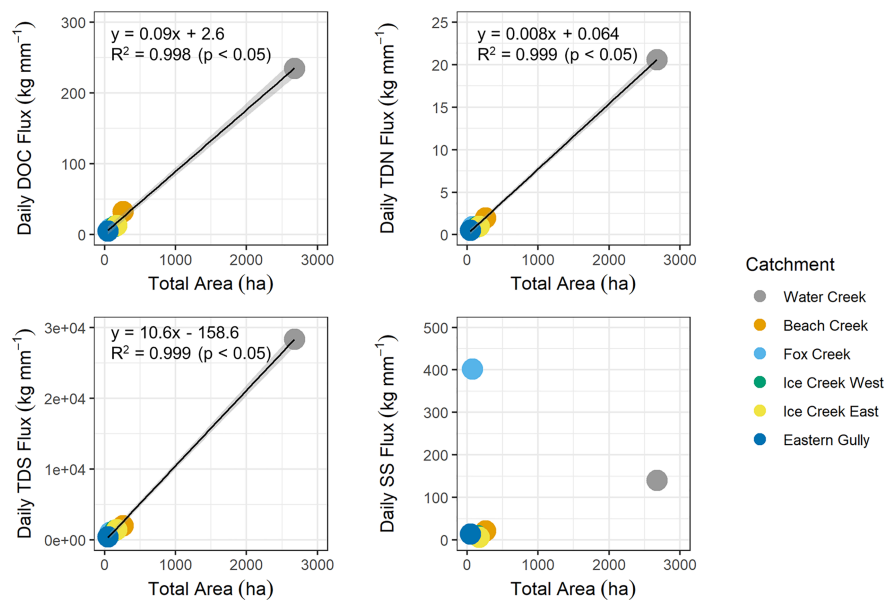


**Figure 6.** Comparison of total catchment area and daily (a) DOC, (b) TDN, (c) TDS, and (d) SS fluxes of the rivers Water Creek, Beach Creek, Fox Creek, Ice Creek West, Ice Creek East, and Eastern Gully. Fox Creek was excluded to compute the regression as a retrogressive thaw slump formed in the catchment. The size of the points in the plot indicate the degree of catchment disturbance.

#### 5.4. Importance of Disturbances for Hydrochemistry

We studied disturbances that occurred in our study area over the past 65 years. We detect an increase in number of disturbances by 66% and a decrease in area by 41% in all watersheds between 1952 and 2015. If we compare 1952 with 2011, the number of disturbances increased by 154% and the aerial extent decreased by 23% (Figure 2). Ramage et al. (2018) investigate aerial coverage and number of RTSs along the Yukon Coast between 1952 and 2011 and show that the total aerial coverage for this time period increased by 14% and the total number of RTSs increased by 73%. However, the aerial extent of active RTSs decreased by 2%. By examining RTSs and ALDs along the coast of Herschel Island between 1952 and 2000, Lantuit and Pollard (2008) noted an increase by 16% in area of total (active and stable) slumps and by 89% in number of slumps. They further found that ALDs increased by 4% in size and by 158% in number. Thus, the increase in number of disturbances that we see in the studied watersheds range in the same order of magnitude as found in other studies. However, we did not find a similar change in size. While the other studies take into account the coast, our study is focused on ALDs and RTSs inland. Disturbances at the coast have a greater exposure of ground ice to the air and the ocean. The relief and the connection to the ocean favor erosion and transport of material, which may allow disturbances on the coast to develop and expand more in size than inland. Kokelj et al. (2013) examined solute concentrations in the subarctic Peel River (Canada) and found that summer  $\text{Na}:\text{SO}_4$  significantly decreased in the past 40 years as a result of RTSs increase. We do not have long-term data for this site, but based on the scientific literature (Lafrenière & Lamoureux, 2019; Lamoureux & Lafrenière, 2017), we assume that past disturbances have influenced hydrochemical composition.

Hydrological connectivity (section 5.2) and the degree of disturbance determine the impact on stream hydrochemistry. Despite affecting concentrations along the longitudinal stream profiles, the disturbances did not impact the overall size—flux relationship for DOC, TDN, and TDS (Figure 6). The exception, Fox Creek, has much higher sediment loads and also shows a different hydrochemical composition. There is a large RTS inside the catchment, which is hydrologically connected to the mainstream and presumably causing this difference. This shows on one hand the importance of material availability through slumping or spatially widespread disturbances, which can impact the overall flux. On the other hand, it emphasizes the importance of hydrological connectivity of the disturbance in order to transport material and impact the hydrochemical composition at the river outflow. This result is in line with Bowden et al. (2008), who

found that a thermokarst gully increased the SSCs to 2 orders of magnitude in the Toolik River (Alaska). Kokelj et al. (2005) studied lake catchments in the Mackenzie Delta Region and found that RTSs occupying an area as little as 2% already modify the lake chemistry. The relative disturbed area for our studied rivers is similarly low (<2%) but mostly composed of ALDs, which do not have the potential to alter overall size-flux relationships in the summer. It is important to bear in mind that increased rainfall events in the future (Bintanja, 2018) might increase hydrological connectivity and thus alter size-flux relationships in the future. Long-term river monitoring across the Arctic will be crucial to understand long-term trends in lateral geochemical fluxes.

## 6. Conclusions

This study investigates the summer hydrological response and hydrochemical variability of small watersheds in a Low Arctic setting that are subject to past and recent permafrost disturbances. Between 1952 and 2015, the total disturbed area decreases by 41%, whereas the total number of disturbances increased by 66% in all six catchments. In relation to their size, the paired watersheds ICW and ICE show the largest impacted area and also the highest number of disturbances.

ICW and ICE exhibit a similar hydrological response with a high storage capacity as supported by runoff ratios between 0.13 and 0.15. The isotopic signature indicates a change of water source between late July to mid-August. The rain signal becomes stronger over the course of the season. We find a linear relationship between catchment size and those hydrochemical fluxes when incorporating data of nearby streams ( $n = 6$ ). Suspended sediment flux is highly variable and is most likely dependent on local sediment sources and hydrological connectivity. ICW carries 32.8 kg/mm and ICE 12.1 kg/mm over the monitoring season.

Although ICE and ICW are adjacent to each other showing a similar hydrological response, different processes are influencing upstream to downstream hydrochemical compositions. DOC concentrations at the outflow are only reflecting the upstream conditions in ICE. In ICW, ice-wedge polygon degradation possibly leads to increased DOC concentrations upstream, which are not reflected downstream. In both creeks, turbidity as a proxy for SSC increases downstream. Turbidity concentrations measured at the outflow reflect sources in close proximity, which may be rapidly exhausted through rainfall events. Hydrological connectivity of disturbances is necessary to transport material out of the watershed. Similarly, connectivity plays an important role for mobilizing solutes. TDS,  $\text{SO}_4^{2-}$ , and  $\text{Na}:\text{SO}_4$  followed different patterns along both streams and are linked to hydrologically connected disturbances. We conclude that concentrations measured at the outflow of a stream do not necessarily reflect the processes in a catchment. However, in our case study, the influence of ice-wedge polygon degradation and local disturbances had not been strong enough to alter the linear size to DOC, TDN, and TDS flux relationship. This study aims at understanding processes controlling hydrochemical variability and will ultimately help to establish a baseline of flux estimates of small rivers to the Arctic Ocean.

## Author Contributions

C. C., H. L. and S. L. developed the study design. Field work was conducted by C. C. in 2016. C. K. ran lab analyzes for POC, DOC, and TDN of the samples. H. M. performed lab analyzes for the stable water isotopes. J. R. mapped the disturbances using aerial photographs and satellite images. C. C. ran lab analyzes, processed all data, and prepared the manuscript with editorial contributions from all coauthors.

## Data Availability Statement

Data has been made available through PANGAEA: Coch, Caroline; Ramage, Justine L; Lamoureux, Scott; Meyer, Hanno; Knoblauch, Christian; Lantuit, Hugues (2018): Hydrochemistry, runoff and mapped disturbances of Low Arctic Watersheds on Herschel Island, Yukon Territory, Canada, in year 2016. PANGAEA (<https://doi.org/10.1594/PANGAEA.893999>).

## Competing Interests

The authors declare that they have no conflict of interest.

## Acknowledgments

We thank the anonymous reviewer and A. Liljedahl, who helped improving the manuscript. We are grateful to the Yukon Territorial Government, Yukon Parks (Herschel Island Qikiqtaryuk Territorial Park), and the Aurora Research Institute for their support during this project. This publication is part of the Nunataryuk project. The project has received funding under the European Union's Horizon 2020 Research and Innovation Programme under Grant Agreement 773421. C. Coch received a scholarship from the Studienstiftung des deutschen Volkes. J. Ramage was supported through a scholarship from Potsdam University. The authors wish to thank A. Eulenburg, M. Weiner, B. Grabellus, M. Jaskólski, N. Mätzing, P. Overduin, J. Schneider, and S. Stettner for their help in the instrumentation setup, data collection in the field, and laboratory analyses. A special thanks to C. Eckert, R. Gordon, R. Joe, P. Lennie, E. McLeod, and S. McLeod for their support and helpful insights in the field. Thanks to G. Hugelius for providing the satellite imagery and to M. Littmann and E. Dunker for constructing the piezometers.

## References

- Abbott, B. W., Jones, J. B., Godsey, S. E., Larouche, J. R., & Bowden, W. B. (2015). Patterns and persistence of hydrologic carbon and nutrient export from collapsing upland permafrost. *Biogeosciences*, *12*(12), 3725–3740. <https://doi.org/10.5194/bg-12-3725-2015>
- Bintanja, R. (2018). The impact of Arctic warming on increased rainfall. *Scientific Reports*, *8*(1), 16001. <https://doi.org/10.1038/s41598-018-34450-3>
- Bintanja, R., & Andry, O. (2017). Towards a rain-dominated Arctic. *Nature Climate Change*, *7*(4), 263–267. <https://doi.org/10.1038/nclimate3240>
- Bolduc, C., Lamoureux, S. F., & Franssen, J. (2018). Thermal and isotopic evidence for surface and subsurface water contributions to baseflow in a high Arctic river. *Hydrological Processes*, *32*(5), 602–616. <https://doi.org/10.1002/hyp.11427>
- Bowden, W. B., Gooseff, M. N., Balsler, A., Green, A., Peterson, B. J., & Bradford, J. (2008). Sediment and nutrient delivery from thermokarst features in the foothills of the North Slope, Alaska: Potential impacts on headwater stream ecosystems. *Journal of Geophysical Research*, *113*, G02026. <https://doi.org/10.1029/2007JG000470>
- Burn, C. R. (2012). *Herschel Island Qikiqtaryuk: A natural and cultural history of Yukon's Arctic Island*. Calgary, Canada: University of Calgary Press.
- Burn, C. R., & Zhang, Y. (2009). Permafrost and climate change at Herschel Island (Qikiqtaruq), Yukon Territory, Canada. *Journal of Geophysical Research*, *114*, F02001. <https://doi.org/10.1029/2008JF001087>
- Carey, S. K., Boucher, J. L., & Duarte, C. M. (2013). Inferring groundwater contributions and pathways to streamflow during snowmelt over multiple years in a discontinuous permafrost subarctic environment (Yukon, Canada). *Hydrogeology Journal*, *21*(1), 67–77. <https://doi.org/10.1007/s10040-012-0920-9>
- CAVM. (2003). Circumpolar Arctic vegetation map. Conservation of Arctic Flora and Fauna (CAFF) Map.
- Coch, C., Juhls, B., Lamoureux, S. F., Lafrenière, M. J., Fritz, M., Heim, B., & Lantuit, H. (2019). Comparisons of dissolved organic matter and its optical characteristics in small low and high Arctic catchments. *Biogeosciences*, *16*, 4535–4553. <https://doi.org/10.5194/bg-16-4535-2019>
- Coch, C., Lamoureux, S. F., Knoblauch, C., Eiseheid, I., Fritz, M., Obu, J., & Lantuit, H. (2018). Summer rainfall DOC, solute and sediment fluxes in a small Arctic coastal catchment on Herschel Island (Yukon Territory, Canada). *Arctic Science*, *4*(4), 750–780. <https://doi.org/10.1139/as-2018-0010>
- Dansgaard, W. (1964). Stable isotopes in precipitation. *Tellus*, *16*(4), 436–468. <https://doi.org/10.1111/j.2153-3490.1964.tb00181.x>
- Dedkov, A. (2004). The relationship between sediment yield and drainage basin area. Paper presented at the Sediment Transfer through the Fluvial System, Moscow, Russia.
- Eiseheid, I. (2015). Mapping of soil organic carbon and nitrogen in two small adjacent Arctic watersheds on Herschel Island, Yukon Territory. (Master Thesis), University of Hohenheim
- Environment and Climate Change Canada. (2018). Environment and Climate Change Canada, Historical Data. Retrieved from [http://climate.weather.gc.ca/historical\\_data/search\\_historic\\_data\\_e.html](http://climate.weather.gc.ca/historical_data/search_historic_data_e.html)
- Favaro, E. A., & Lamoureux, S. F. (2014). Antecedent controls on rainfall runoff response and sediment transport in a High Arctic catchment. *Geografiska Annaler: Series A, Physical Geography*. <https://doi.org/10.1111/geoa.12063>
- Favaro, E. A., & Lamoureux, S. F. (2015). Downstream patterns of suspended sediment transport in a High Arctic river influenced by permafrost disturbance and recent climate change. *Geomorphology*, *246*, 359–369. <https://doi.org/10.1016/j.geomorph.2015.06.038>
- Fouché, J., Lafrenière, M. J., Rutherford, K., & Lamoureux, S. (2017). Seasonal hydrology and permafrost disturbance impacts on dissolved organic matter composition in High Arctic headwater catchments. *Arctic Science*, *3*(2), 378–405. <https://doi.org/10.1139/as-2016-0031>
- Freeze, R. A., & Cherry, J. A. (1979). *Groundwater*. Englewood Cliffs, NJ: Prentice-Hall.
- Frey, K. E., & McClelland, J. W. (2009). Impacts of permafrost degradation on Arctic river biogeochemistry. *Hydrological Processes*, *23*(1), 169–182. <https://doi.org/10.1002/hyp.7196>
- Fritz, M., Wetterich, S., Meyer, H., Schirrmeyer, L., Lantuit, H., & Pollard, W. H. (2011). Origin and characteristics of massive ground ice on Herschel Island (western Canadian Arctic) as revealed by stable water isotope and hydrochemical signatures. *Permafrost and Periglacial Processes*, *22*(1), 26–38. <https://doi.org/10.1002/ppp.714>
- IAEA/WMO. (2018). Global network of isotopes in precipitation. The GNIP database. Retrieved from <http://www.iaea.org/water>
- IPCC (2013). In T. F. Stocker, D. Qin, G.-K. Plattner, M. Tignor, S. K. Allen, J. Boschung, A. Nauels, Y. Xia, V. Bex, & P. M. Midgley (Eds.), *The physical science basis. Contribution of Working Group I to the Fifth Assessment Report of the Intergovernmental Panel on Climate Change* (p. 1535). Cambridge, UK and New York, NY: Cambridge University Press. C. U. Press Ed.
- Irrgang, A. M., Lantuit, H., Manson, G. K., Günther, F., Grosse, G., & Overduin, P. P. (2018). Variability in rates of coastal change along the Yukon Coast, 1951 to 2015. *Journal of Geophysical Research: Earth Surface*, *123*, 779–800. <https://doi.org/10.1002/2017JF004326>
- Kokelj, S. V., Jenkins, R. E., Milburn, D., Burn, C. R., & Snow, N. (2005). The influence of thermokarst disturbance on the water quality of small upland lakes, Mackenzie Delta region, Northwest Territories, Canada. *Permafrost and Periglacial Processes*, *16*(4), 343–353. <https://doi.org/10.1002/ppp.536>
- Kokelj, S. V., Lacelle, D., Lantz, T. C., Tunnicliffe, J., Malone, L., Clark, I. D., & Chin, K. S. (2013). Thawing of massive ground ice in mega slumps drives increases in stream sediment and solute flux across a range of watershed scales. *Journal of Geophysical Research: Earth Surface*, *118*, 681–692. <https://doi.org/10.1002/jgrf.20063>
- Kokelj, S. V., Lantz, T. C., Wolfe, S. A., Kanigan, J. C., Morse, P. D., Coutts, R., et al. (2014). Distribution and activity of ice wedges across the forest-tundra transition, western Arctic Canada. *Journal of Geophysical Research: Earth Surface*, *119*, 2032–2047. <https://doi.org/10.1002/2014JF003085>
- Lacelle, D., Björnson, J., & Lauriol, B. (2010). Climatic and geomorphic factors affecting contemporary (1950–2004) activity of retrogressive thaw slumps on the Aklavik Plateau, Richardson Mountains, NWT, Canada. *Permafrost and Periglacial Processes*, *21*(1), 1–15. <https://doi.org/10.1002/ppp.666>
- Lafrenière, M. J., & Lamoureux, S. F. (2013). Thermal perturbation and rainfall runoff have greater impact on seasonal solute loads than physical disturbance of the active layer. *Permafrost and Periglacial Processes*, *24*(3), 241–251. <https://doi.org/10.1002/ppp.1784>
- Lafrenière, M. J., & Lamoureux, S. F. (2019). Effects of changing permafrost conditions on hydrological processes and fluvial fluxes. *Earth-Science Reviews*, *191*, 212–223. <https://doi.org/10.1016/j.earscirev.2019.02.018>
- Lamhonwah, D., Lafrenière, M. J., Lamoureux, S. F., & Wolfe, B. B. (2017). Evaluating the hydrological and hydrochemical responses of a High Arctic catchment during an exceptionally warm summer. *Hydrological Processes*, *31*(12), 2296–2313. <https://doi.org/10.1002/hyp.11191>

- Lamoureux, S. F., & Lafrenière, M. J. (2009). Fluvial impact of extensive active layer detachments, Cape Bounty, Melville Island, Canada. *Arctic, Antarctic, and Alpine Research*, 41(1), 59–68. [https://doi.org/10.1657/1938-4246\(08-030\)\[lamoureux\]2.0.co;2](https://doi.org/10.1657/1938-4246(08-030)[lamoureux]2.0.co;2)
- Lamoureux, S. F., & Lafrenière, M. J. (2017). More than just snowmelt: Integrated watershed science for changing climate and permafrost at the Cape Bounty Arctic Watershed Observatory. *Wiley Interdisciplinary Reviews: Water*, 5(1), e1255. <https://doi.org/10.1002/wat2.1255>
- Lamoureux, S. F., & Lafrenière, M. J. (2018). More than just snowmelt: Integrated watershed science for changing climate and permafrost at the Cape Bounty Arctic Watershed Observatory. *Wiley Interdisciplinary Reviews: Water*, 5(1), e1255. <https://doi.org/10.1002/wat2.1255>
- Lantuit, H., & Pollard, W. H. (2008). Fifty years of coastal erosion and retrogressive thaw slump activity on Herschel Island, southern Beaufort Sea, Yukon Territory, Canada. *Geomorphology*, 95(1–2), 84–102. <https://doi.org/10.1016/j.geomorph.2006.07.040>
- Laudon, H., Köhler, S., & Buffam, I. (2004). Seasonal TOC export from seven boreal catchments in northern Sweden. *Aquatic Sciences - Research Across Boundaries*, 66(2), 223–230. <https://doi.org/10.1007/s00027-004-0700-2>
- Lewkowicz, A. G. (2007). Dynamics of active-layer detachment failures, Fosheim Peninsula, Ellesmere Island, Nunavut, Canada. *Permafrost and Periglacial Processes*, 18(1), 89–103. <https://doi.org/10.1002/ppp.578>
- Liljedahl, A. K., Boike, J., Daanen, R. P., Fedorov, A. N., Frost, G. V., Grosse, G., et al. (2016). Pan-Arctic ice-wedge degradation in warming permafrost and its influence on tundra hydrology. *Nature Geoscience*, 9(4), 312–318. <https://doi.org/10.1038/ngeo2674>
- Mackay, J. R. (1959). Glacier ice-thrust features of the Yukon coast. *Geographical Bulletin*, 13, 5–21.
- Meyer, H., Schönicke, L., Wand, U., Hubberten, H. W., & Friedrichsen, H. (2000). Isotope studies of hydrogen and oxygen in ground ice-experiences with the equilibration technique. *Isotopes in Environmental and Health Studies*, 36(2), 133–149. <https://doi.org/10.1080/10256010008032939>
- Myers-Smith, I. H., Hik, D. S., Kennedy, C., Cooley, D., Johnstone, J. F., Kenney, A. J., & Krebs, C. J. (2011). Expansion of canopy-forming willows over the twentieth century on Herschel Island, Yukon Territory, Canada. *Ambio*, 40(6), 610–623. <https://doi.org/10.1007/s13280-011-0168-y>
- Obu, J., Lantuit, H., Myers-Smith, I., Heim, B., Wolter, J., & Fritz, M. (2017). Effect of terrain characteristics on soil organic carbon and total nitrogen stocks in soils of Herschel Island, Western Canadian Arctic. *Permafrost and Periglacial Processes*, 28(1), 92–107. <https://doi.org/10.1002/ppp.1881>
- Osterkamp, T. E. (2007). Characteristics of the recent warming of permafrost in Alaska. *Journal of Geophysical Research*, 112, F02S02. <https://doi.org/10.1029/2006JF000578>
- Petrone, K. C., Jones, J. B., Hinzman, L. D., & Boone, R. D. (2006). Seasonal export of carbon, nitrogen, and major solutes from Alaskan catchments with discontinuous permafrost. *Journal of Geophysical Research*, 111, G02020. <https://doi.org/10.1029/2005JG000055>
- Radosavljevic, B., Lantuit, H., Pollard, W., Overduin, P., Couture, N., Sachs, T., et al. (2015). Erosion and flooding—Threats to coastal infrastructure in the Arctic: A case study from Herschel Island, Yukon Territory, Canada. *Estuaries and Coasts*, 39(4), 900–915. <https://doi.org/10.1007/s12237-015-0046-0>
- Ramage, J. L., Irrgang, A. M., Herzsuh, U., Morgenstern, A., Couture, N., & Lantuit, H. (2017). Terrain controls on the occurrence of coastal retrogressive thaw slumps along the Yukon Coast, Canada. *Journal of Geophysical Research: Earth Surface*, 122, 1619–1634. <https://doi.org/10.1002/2017JF004231>
- Ramage, J. L., Irrgang, A. M., Morgenstern, A., & Lantuit, H. (2018). Increasing coastal slump activity impacts the release of sediment and organic carbon into the Arctic Ocean. *Biogeosciences*, 15(5), 1483–1495. <https://doi.org/10.5194/bg-15-1483-2018>
- Rampton, V. N. (1982). *Quaternary geology of the Yukon Coastal Plain* (p. 49). Ottawa, Canada: Geological Survey of Canada.
- Schuur, E. A. G., Crummer, K. G., Vogel, J. G., & Mack, M. C. (2007). Plant species composition and productivity following permafrost thaw and thermokarst in Alaskan Tundra. *Ecosystems*, 10(2), 280–292. <https://doi.org/10.1007/s10021-007-9024-0>
- Singh, V. (1992). *Elementary hydrology*. Englewood Cliffs, NJ: Prentice Hall.
- Skogerboe, G. V., Walker, W. R., & Bennett, R. S. (1973). Generalized discharge relations for cutthroat flumes. *Journal of the Irrigation and Drainage Division*, 98(4), 569–583. <https://doi.org/10.13031/2013.37449>
- Smith, C. A. S., Kennedy, C. E., Hargrave, A. E., & McKenna, K. M. (1989). *Soil and vegetation of Herschel Island, Yukon Territory*. ON: Retrieved from Ottawa.
- Tank, S. E., Fellman, J. B., Hood, E., & Kritzbeg, E. S. (2018). Beyond respiration: Controls on lateral carbon fluxes across the terrestrial-aquatic interface. *Limnology and Oceanography Letters*, 3(3), 76–88. <https://doi.org/10.1002/lol2.10065>
- Tanski, G., Couture, N., Lantuit, H., Eulenburg, A., & Fritz, M. (2016). Eroding permafrost coasts release low amounts of dissolved organic carbon (DOC) from ground ice into the nearshore zone of the Arctic Ocean. *Global Biogeochemical Cycles*, 30, 1054–1068. <https://doi.org/10.1002/2015GB005337>
- Vonk, J. E., Mann, P. J., Dowdy, K. L., Davydova, A., Davydov, S. P., Zimov, N., et al. (2013). Dissolved organic carbon loss from Yedoma permafrost amplified by ice wedge thaw. *Environmental Research Letters*, 8(3). <https://doi.org/10.1088/1748-9326/8/3/035023>
- Vonk, J. E., Tank, S. E., Bowden, W. B., Laurion, I., Vincent, W. F., Alekseychik, P., et al. (2015). Reviews and syntheses: Effects of permafrost thaw on Arctic aquatic ecosystems. *Biogeosciences*, 12(23), 7129–7167. <https://doi.org/10.5194/bg-12-7129-2015>
- Wegner, C., Bennett, K. E., de Vernal, A., Forwick, M., Fritz, M., Heikkilä, M., et al. (2015). Variability in transport of terrigenous material on the shelves and the deep Arctic Ocean during the Holocene. *Polar Research*, 34(1), 24964. <https://doi.org/10.3402/polar.v34.24964>
- Woo, M. (2012). *Permafrost hydrology*. Heidelberg: Springer.
- Woo, M.-K., Kane, D. L., Carey, S. K., & Yang, D. (2008). Progress in permafrost hydrology in the new millennium. *Permafrost and Periglacial Processes*, 19(2), 237–254. <https://doi.org/10.1002/ppp.613>
- Zolkos, S., Tank, S. E., & Kokelj, S. V. (2018). Mineral weathering and the permafrost carbon-climate feedback. *Geophysical Research Letters*, 45, 9623–9632. <https://doi.org/10.1029/2018GL078748>